Comparison of the electrochemical properties of impregnated and functionally gradient LaNi$_{0.6}$Fe$_{0.4}$O$_3$–Gd$_{0.2}$Ce$_{0.8}$O$_2$ composite cathodes for Solid Oxide Fuel Cell

Bo Huang [a],[*], Xin-jian Zhu [a], Huai-wen Nie [b], Ya-ran Niu [b], Yang Li [a], Nian Cheng [a]

[a] Institute of Fuel Cell, School of Mechanical Engineering, Shanghai Jiaotong University, 800 Dongchuan Road, Shanghai 200240, PR China
[b] CAS Key Laboratory of Materials for Energy Conversion, Shanghai Institute of Ceramics, Chinese Academy of Sciences (SICCAS), 1295 Dingxi Road, Shanghai 200050, PR China

HIGHLIGHTS

► Functionally gradient LNF cathode changes in composite between ScSZ and LNF.
► Functionally gradient LNF cathode shows better performance than that of LNF–GDC.
► Impregnation of nano-sized GDC in LNF porous network can substantially enhance TPBs.
► GDC-impregnated LNF cathode shows the lowest specific polarization resistance.

ARTICLE INFO

ABSTRACT

This study investigates the electrochemical properties of three different configurations of LaNi$_{0.6}$Fe$_{0.4}$O$_3$ (LNF)-based cathodes for Solid Oxide Fuel Cell (SOFC). The results show functionally gradient LNF cathode and Gd$_{0.2}$Ce$_{0.8}$O$_2$ (GDC)-impregnated LNF cathode both reveal the better electrochemical properties compared to that of 70 wt.% LNF–30 wt.% GDC cathode. Functionally gradient LNF cathode with better interface of LNF/GDC/ScSZ can be achieved by the gradual change in composition from electrolyte to cathode, resulting in the decline in charge transfer resistance and gas phase diffusion resistance, therefore the decline in specific cathode polarization resistance (R_p). Whereas, the dramatic decrease in R_p for GDC-impregnated LNF cathode is mainly attributed to the extended triple phase boundary (TPB) and enhanced oxide ion conductivity. The nano-sized GDC particle on LNF backbone with high porosity would allow gas phase molecules to easily diffuse to the LNF/GDC/ScSZ boundaries, which significantly enhances cathode activities for oxygen reduction reaction (ORR). The GDC-impregnated LNF cathode reveals the lowest R_p, the lowest activation energies of R_p and the lowest activation energy of ORR among three cathode configurations. Noticeably, the cathode performance can be significantly improved by impregnating nano-sized GDC particles into LNF porous backbone.
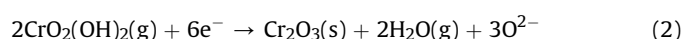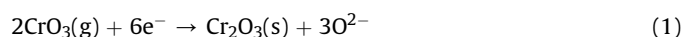
1. Introduction

Reducing the operating temperature of Solid Oxide Fuel Cell (SOFC) down to 600–800 °C brings both dramatic economic and technical benefits. The cost of SOFC technology may be dramatically reduced since much less expensive materials can be used in cell construction and novel fabrication techniques can be applied to the stack and system integration. Further, the reduction in the operating temperature would greatly reduce the degradation of SOFC components, widen the materials selection, lessen the sealing problem, allow the use of metallic materials as the interconnects, and eventually accelerate the commercialization of SOFC technology.

However, the performance of an SOFC system would decrease because of the low oxide ion conductivity of yttria-stabilized zirconia (YSZ), the high overpotential at the electrode and the increased polarization resistance of the electrodes, especially for the O$_2$ reduction reaction (ORR) on the cathode side at lower operating temperature. The reduction of the thickness of the YSZ electrolyte [1], and the application of the La(Sr)Ga(Mg)O$_{3-\delta}$ (LSGM) [2–4] or gadolinium-doped ceria (GDC) [5] electrolyte material with higher ionic conductivity than YSZ, has all significantly reduced the ohmic loss from the electrolyte. However, the conventional SOFC cathode, strontium-doped lanthanum manganite (LSM), is not suitable for IT-SOFC due to its low activity below 800 °C [6]. Noticeably, Cr poisoning is most significant in the LSM cathode. For instance, a layer of chromium oxide (Cr$_2$O$_3$) formed on the surface of the Cr-containing alloy interconnect after long-time operation results in high electrical resistance which degrades SOFC performance [7,8].

* Corresponding author. Tel./fax: +86 21 34206249.
E-mail address: huangbo2k@hotmail.com (B. Huang).

Furthermore, on the cathode side, Cr_2O_3 can react with oxygen and moisture to form volatile Cr species in oxidizing atmospheres under SOFC operating temperatures [9–12]. Among several kinds of volatile Cr species, $CrO_3(g)$ and $CrO_2(OH)_2(g)$ are considered as high vapor pressure phases [10,13]. Thus a number of Cr(6+) species such as $CrO_3(g)$ and $CrO_2(OH)_2(g)$ have significant vapor pressure above $Cr_2O_3(s)$ in moist air. These species would freely move around. A sufficient quantity would migrate through the porous structure of the cathode and reach the cathode/electrolyte interface. The normal process at the cathode/electrolyte interface is the O_2 reduction reaction $O_2 + 4e^- \rightarrow 2O^{2-}$. Similarly, other oxides in the vapor form which can supply oxygen at the interface can be easily reduced. Thus, when $CrO_2(OH)_2$ and CrO_3 reach the oxide ion-conducting media (electrolyte) and an electrically conducting phase (cathode), the following reactions for $CrO_2(OH)_2(g)$ and $CrO_3(g)$ are likely to compete with the normal O_2 reduction process [14]:

$$2CrO_3(g) + 6e^- \rightarrow Cr_2O_3(s) + 3O^{2-} \tag{1}$$

$$2CrO_2(OH)_2(g) + 6e^- \rightarrow Cr_2O_3(s) + 2H_2O(g) + 3O^{2-} \tag{2}$$

Cr^{6+} can be readily reduced to Cr^{3+}, electrochemically forming Cr_2O_3 and releasing water and an oxide ion at the cathode/electrolyte interface. Therefore, in the case of $CrO_2(OH)_2(g)$ and $CrO_3(g)$, unlike the O_2 reduction reaction, a significant amount of residue in the form of $Cr_2O_3(s)$ is left behind at the cathode/electrolyte interface. Another possible cause for $Cr_2O_3(s)$ deposition at the cathode/electrolyte interface may be indirectly related to the oxygen reduction reaction [14,15]. Since the reaction $2CrO_3(g) \rightarrow Cr_2O_3(s) + 1.5O_2$ is driven by the oxygen partial pressure at a constant temperature, the deposition of $Cr_2O_3(s)$ at or near the interface can also occur due to the lower oxygen partial pressure at the cathode/electrolyte interface compared to that in the bulk gas phase, which is also possible in a cell polarized with large current densities. The $Cr_2O_3(s)$ deposited at or near the interface by either of the mechanisms discussed above then can easily react with LSM to form the $(Cr,Mn)_3O_4(s)$ spinel phase and $(LaSr)(MnCr)O_3$, eventually leading to cathodic polarization loss and to rapid performance degradation of the SOFC. It is also reported that the deposition process is most likely limited by the nucleation reaction between these Cr species and the nucleation agents such as manganese species (Mn^{2+}) generated from LSM under the cathodic polarization in the LSM cathode–zirconia electrolyte system [16]. Mn^{2+} ions on the LSM surface can react with the Cr species and forms the Cr–Mn–O nuclei and, subsequently, $(Cr,Mn)_3O_4(s)$ [14,17]. The $(La,Sr)(Co,Fe)O_3$ (LSCF) is known to be a very good mixed ionic and electronic conductor with high electrocatalytic activity for the O_2 reduction reactions at lower temperature [18]. Unfortunately, volatile Cr species are generated over the chromia scale of chromia-forming alloy interconnect, forming $SrCrO_4$ on the porous LSCF surface [19], poisoning the LSCF cathode and causing the rapid degradation of the cell performance. Thus, SOFC based on the chromia-forming alloy interconnect requires the development of the cathode materials not only with the high electrocatalytic activity but also with the high Cr-tolerance. Systematic studies have also shown that the interaction between the Cr species and cathodes is strongly dependent on the nature of the cathode materials [20], which suggests the possibility to develop stable cathode materials with high tolerance to Cr poisoning by proper cathode composition, i.e., without a nucleation agent for Cr deposition.

Recently, La(Ni,Fe)O$_3$ perovskite material has been developed as one of the most promising cathode materials in IT-SOFC operated at 600–800 °C. Of particular interest is $LaNi_{0.6}Fe_{0.4}O_3$ (LNF) which exhibits high electronic conductivity, a thermal expansion coefficient close to that of the zirconia electrolyte, high electrochemical activity

for the oxygen reduction reaction, and resistance to cathode poisoning by chromia vapor from the metal separators [21–24]. However, the initial performance of the LNF cathode is not very high. More than 100 h is required for the cathode to reach a stable state at which point the LNF cathode exhibits very high levels of performance [25]. This characteristic is a disadvantage as regards the practical applications. It must be improved if we will apply LNF cathode material to practical SOFC, since SOFC must generate a certain amount of power from the beginning at lower temperature. On one hand, LNF is more reactive with ZrO_2-based electrolyte than conventional La(Sr)MnO$_3$ in the sintering temperature region [25,26], resulting in the formation of $La_2Zr_2O_7$ with low electronic and ionic conductivity. The poor performance of the LNF cathode prior to the current loading is considered to be associated with the $La_2Zr_2O_7$ formation [27,28]. Some studies have suggested that the effect of a $La_2Zr_2O_7$ layer can be reduced by applying current loading to the cell [23,27,28]. On the other hand, the polarization resistance of LNF cathode increased with time without a significant change in the ohmic resistance. According to Ref. [29], the increase of polarization resistance with time could be explained by reoxidation of sintered LNF material and consequent decrease of oxygen vacancy concentration. It is noted that the LNF cathodes tend to lose oxygen on heating, resulting in oxygen vacancy formation [30]. In recent years, potential cathode candidates have normally been based on mixed oxygen ionic and electronic conducting oxides, which have both high ionic and electronic conductivity, and have attracted a lot of attention in terms of their applications for fuel cell electrodes, oxygen separator membranes and membrane reactors for the partial oxidation of methane to syngas [31–33]. The mixed conductivity extends the active oxygen reduction sites from the typical electrolyte–electrode–gas triple phase boundary to the entire cathode surface, therefore greatly reducing the cathode polarization at low operating temperatures [34]. In particular, gadolinia-doped ceria (GDC) is a candidate material for this application. Typically, the ionic conductivity of GDC is of the order of magnitude of 50×10^{-3} S cm^{-1} at SOFC operating temperatures (600–800 °C) [35–37]. This is higher than the typical corresponding ionic conductivity of YSZ [38]. The difference is more pronounced at lower temperatures, e.g. at 700 °C the conductivity of GDC is 5.8×10^{-3} S cm^{-1} as compared to 1.4×10^{-4} S cm^{-1} for YSZ.

In this study, we employed two potential methods to improve the LNF cathode performance. The first approach is functionally gradient cathodes which were used to reduce the cathode polarization resulting from the incompatibility between the cathode and the electrolyte. The functionally graded materials (FGMs) were used to reduce the cathode polarization. FGMs have been developed as a method of joining dissimilar materials that are usually incompatible [39]. Instead of an abrupt change in composition and/or microstructure between the two materials, FGMs have a graded interface at which the composition gradually changes from one material to the other. The novelty of this study is in its application of the functionally gradient materials concept to the LNF cathode. Namely, this study investigated the electrochemical performance of gradient LNF composite cathodes on ScSZ electrolyte. Another potential approach is ion impregnation that can be achieved by firing the two phases at different temperatures, unlike conventional co-fired composite electrodes. The technique involves depositing nanoparticles into a pre-sintered backbone. The sintering of backbone is performed at high temperature, which ensures good bonding between the electrode backbone and the electrolyte, good connection between the particles to achieve high effective conduction of electron or oxygen ion, and the structural stability of the cathode. The firing process for the deposition of nanoparticles and the formation of the desired phase can be conducted at temperature much lower than that needed for the traditional ceramic

fabrication process. The impregnation may also alleviate the thermal expansion mismatch problems. In a cathode fabricated by the impregnation process, the coefficient of thermal expansion (CTE) is dominated by the backbone materials, and impregnation the CTE mismatched materials has little effect on the CTE of the electrode. Depositing active nanoparticles onto a porous electrode backbone by impregnation has been proven to be a facile and effective approach for electrochemical performance enhancement due to relatively low area specific resistances [40—43]. In this paper, the electrochemical properties of three different configurations (i.e., composite LNF-based cathode (70 wt.% LNF—30 wt.% GDC), functionally gradient LNF cathode, and GDC-impregnated LNF cathode) were investigated systematically.

2. Experimental

2.1. Fabrication of symmetrical cell

The composition of La(Ni,Fe)O_3-based cathode was chosen as $LaNi_{0.6}Fe_{0.4}O_{3-\delta}$ (LNF) [17,19]. The LNF cathode material was prepared using a combustion synthesis technique described elsewhere [44]. The polarization resistance of the LNF cathode was measured in the two-electrode symmetric cell configuration under air [45]. ScSZ (scandia-stabilized zirconia, $Sc_{0.1}Zr_{0.9}O_{1.95}$, 99.99% pure, Daiichi Kigenso, Japan) pellet with the diameter of 20 mm and the thickness of about 200 μm was used as the electrolyte. The both sides of the ScSZ electrolyte pellet were subsequently covered with a 2 μm thick $Gd_{0.2}Ce_{0.8}O_2$ (GDC) barrier layer by means of screen printing followed by sintering at 1300 °C for 1 h. Electrolyte-supported symmetric cell for impedance testing was fabricated by screen printing method. The composite cathode was prepared by mixing the LNF cathode with GDC powders using ball milling. The slurry of the cathode powder, which was ground and mixed with isopropyl alcohol, was screen-printed onto both sides of the ScSZ electrolyte pellet. Then the symmetric cell was sintered at 1050 °C for 2 h under stagnant air. After being sintered, the resulting cathode areas are 1 cm^2. The cathode is a circle in shape. The radius of the circle is 0.565 cm. The three different configurations of cathodes in this study are schematically illustrated in Fig. 1, and the compositions of three cathode samples are summarized in Table 1. For the preparation of the functionally gradient LNF cathode, the first layer attached on the ScSZ electrolyte is composed of 60 wt.% LNF + 40 wt.% GDC, the second one is composed of 70 wt.% LNF + 30 wt.% GDC, and the top layer consists of 100 wt.% LNF. For the preparation of the GDC-impregnated LNF, stoichiometric amounts of gadolinium nitrate ($Gd(NO_3)_3 \cdot 6H_2O$) and cerium nitrate ($Ce(NO_3)_3 \cdot 6H_2O$) were dissolved in distilled water with constant stirring. Then, a stoichiometric amount of citric acid ($C_6H_8O_7 \cdot H_2O$), which is a chelating agent and fuel, was also dissolved in this solution. The stoichiometric ratio of citric acid to nitrates was calculated according to Jain et al. [46]. The Ce^{3+} concentration in the transparent solution was 0.4 M. The solution pH was maintained between 7 and 8. The LNF cathode layers of electrolyte-supported symmetric cell sintered at 1050 °C were completely dipped in the above solution and evacuated using a vacuum pump set to an absolute pressure of 200 mbar so that the solution filled the pores of the LNF cathode layer. Then it was dried at 75 °C, followed by calcination at 600 °C for 2 h to decompose $Gd_{0.2}Ce_{0.8}(NO_3)_x$ nitrate solution, forming $Gd_{0.2}Ce_{0.8}O_2$ (GDC) oxide phase. This procedure was repeated several times to have a uniform and sufficient coating. The impregnated GDC loading in the LNF cathode was estimated from the weight change of the LNF cathode coating before and after the impregnation treatment. The loading of GDC was about 21.1 wt.% after repeating the impregnation processes five times. Preparation methods for GDC-impregnated LNF cathode have been described previously [44]. Unless otherwise mentioned,
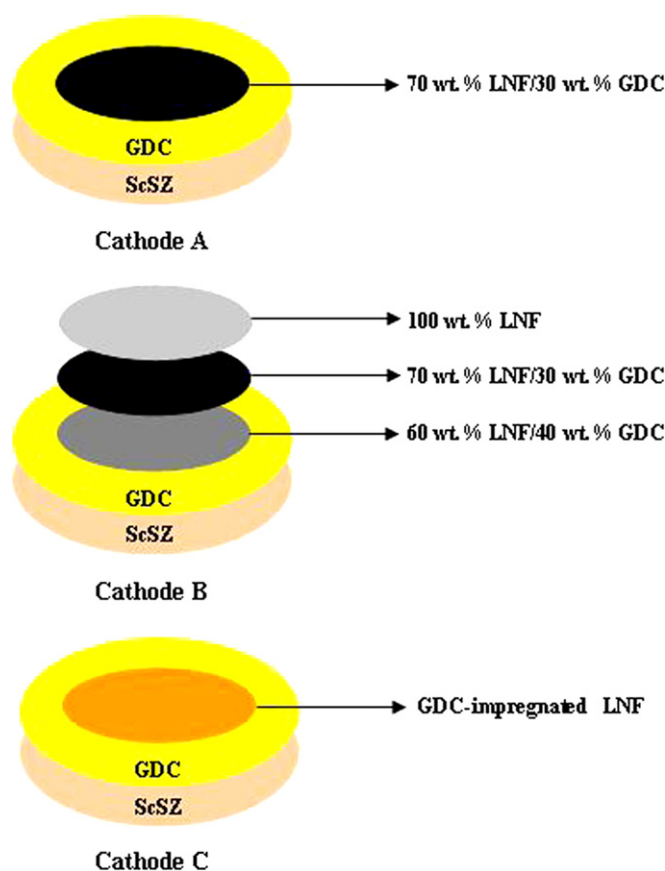

Fig. 1. Schematic diagram of one side of the symmetric cell structure for cathode A, cathode B, and cathode C.

we studied the electrochemical performance of 21.1 wt.% GDC-impregnated LNF cathode in this paper. X-ray diffraction (XRD) patterns were collected with a Philips X'Pert Pro diffractometer equipped with a primary monochromator (Cu Kα radiation) and a Philips X'Celerator detector for the structural characterization of the LNF and GDC powder. The scans were performed in the 2θ range 10—90° at the scanning speed of 4° min^{-1}. Further XRD studies were also carried out to investigate the chemical compatibility of LNF with GDC material. Powder mixture of LNF with ScSZ, in a 1:1 (wt.%) ratio, were ground in an agate mortar and fired at 1100 °C for 5 h. Field emission scanning electron microscope (FE-SEM) images of the gradient LNF—GDC composite cathodes and GDC-impregnated LNF cathodes were analyzed using a microscope (FE-SEM, PHILIPS 515, The Netherlands) equipped with an X-ray analyzer for energy-dispersive X-ray spectroscopy (EDS).

2.2. Electrochemical measurements

The electrochemical activity of the gradient LNF—GDC composite cathodes and GDC-impregnated LNF cathodes was characterized by the electrochemical impedance spectroscopy (EIS), using

Table 1
Summary of three configuration cathode samples.

Sample	Compositions		
	Layer 1	Layer 2	Layer 3
Cathode A	70 wt.% LNF/30 wt.% GDC	70 wt.% LNF/30 wt.% GDC	100 wt.% LNF
Cathode B	60 wt.% LNF/40 wt.% GDC		
Cathode C	GDC-impregnated LNF		

a Solartron 1260 frequency response analyzer at open circuit. The applied frequency was in the range of 0.01 Hz–100 kHz at five points per frequency decade with the signal amplitude of 20 mV. The EIS measurement was carried out in the temperature range of 650–850 °C in steps of 50 °C in the air. To stabilize the cathode behavior, the cathodes were polarized at 750 °C with a constant current density of 100 mA cm^{-2} for 2 h before the electrochemical testing. The EIS fitting analysis was performed with Zview software. The specific ohmic resistance (R_{Ω}) was estimated from the high-frequency intercept of the impedance curves and the specific polarization resistance (R_p) was directly measured from the differences between the low- and high-frequency intercepts on the impedance curves.

3. Results and discussion

The investigation of the solid-state reactions between LNF and GDC phases is very important for evaluating the cathode polarization resistance of LNF–GDC composite cathodes. Fig. 2 shows the XRD patterns of 50 wt.% LNF + 50 wt.% GDC calcined at 1100 °C for 5 h. Pure LNF contains a perovskite structure, while GDC contains a cubic fluorite-type structure. The results reveal that no obvious interface reaction appeared for LNF + GDC composites when heated up to 1100 °C for 5 h and agree with those of Chiba [21]. The LNF material is a chemically stable cathode material for ScSZ electrolyte-based SOFC when the calcined temperature was below 1100 °C [44]. Therefore, in this study, the LNF–GDC composite is also a chemically stable cathode material for ScSZ electrolyte-based SOFC when the calcined temperature is below 1100 °C. In general, a composite cathode material sintered at high temperature with a larger grain size leads to a decrease in the number of the cathode–

electrolyte–gas interface (triple phase boundary, TPB) sites, which results in high polarization resistance [47,48]. Meanwhile, due to the high sintering temperature, the cathode materials adhere strongly to the electrolyte surface, resulting in better contact with the electrolyte and better current collection. This represents a trade-off relationship with regard to the sintering temperature to obtain cathode materials with fine microstructure and strong adhesion to the electrolyte.

Fig. 3(a) shows the microstructure of composite LNF-based cathode (70 LNF–30 GDC) with weight ratio of LNF:GDC being 70:30, which revealed the uniform grains size of LNF are in the range of 0.4–1.0 μm. While, agglomeration phenomenon of GDC particles was observed, the particle size distribution was in the range of 0.1–0.3 μm. After the ion impregnation with $Gd_{0.2}Ce_{0.8}(NO_3)_x$ solution, nanosize GDC particles were introduced to the LNF backbone as shown in Fig. 3(b). The GDC particles were relatively uniform and the grain size was in the range of 40–50 nm, as estimated from the enlarged SEM pictures (Fig. 3(b)). Clearly, the impregnated GDC particles are much smaller than that of LNF particles.

The typical impedance spectroscopies for the LNF-based cathodes are investigated based on a symmetrical cell sintered at 1050 °C for 2 h and recorded under open-circuit conditions in the temperature range of 650–850 °C in air, which are shown in Fig. 4(a)–(e). In this study, we used an equivalent circuit to
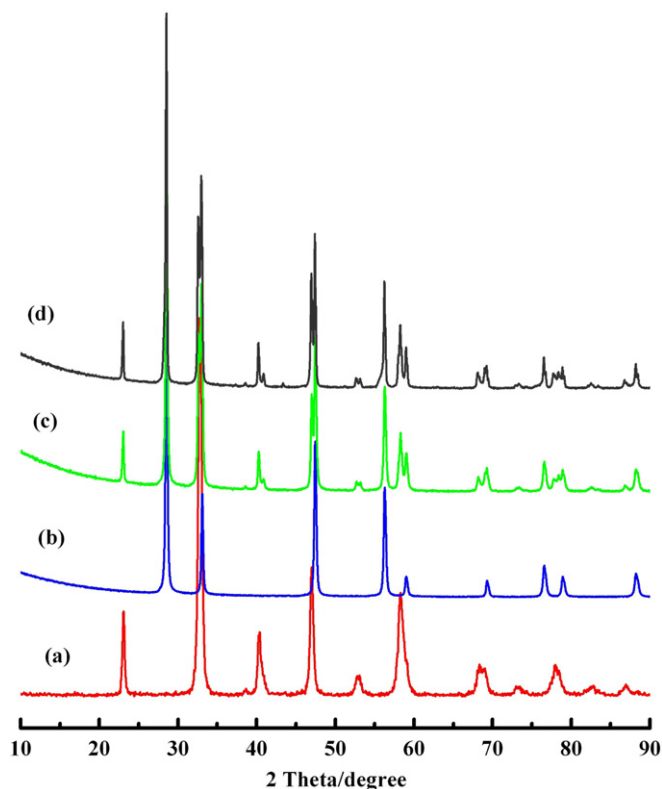

Fig. 2. X-ray diffraction pattern of the powder of (a) LNF, (b) GDC, (c) 50 wt.% LNF + 50 wt.% GDC at room temperature and (d) 50 wt.% LNF + 50 wt.% GDC calcined at 1100 °C for 5 h.

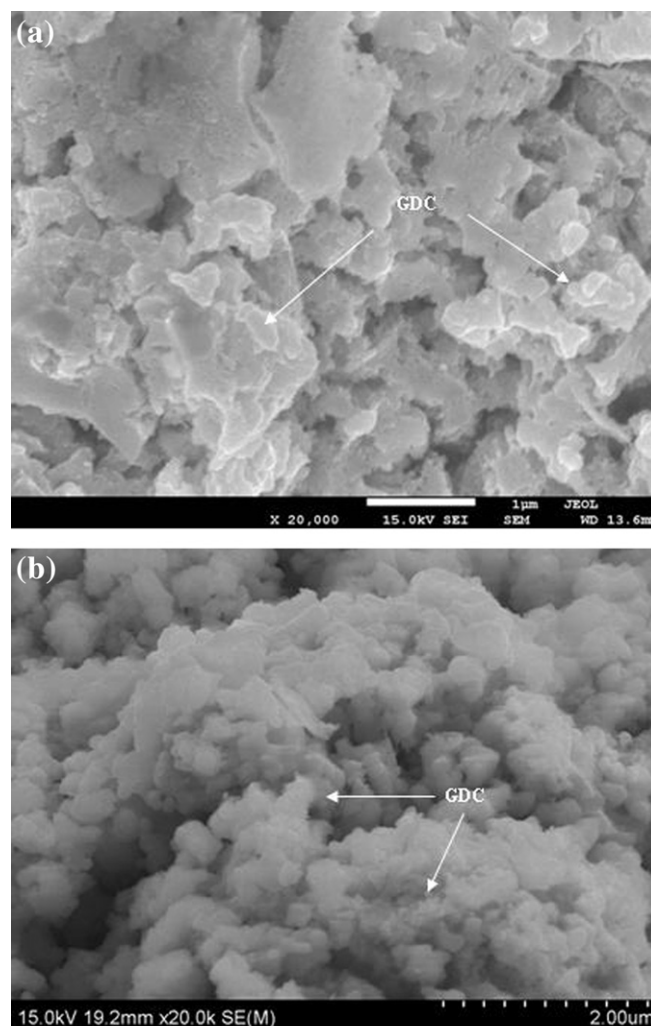Fig. 3. SEM images of (a) composite LNF-based cathode (70 wt.% LNF:30 wt.% GDC) and (b) GDC-impregnated LNF.
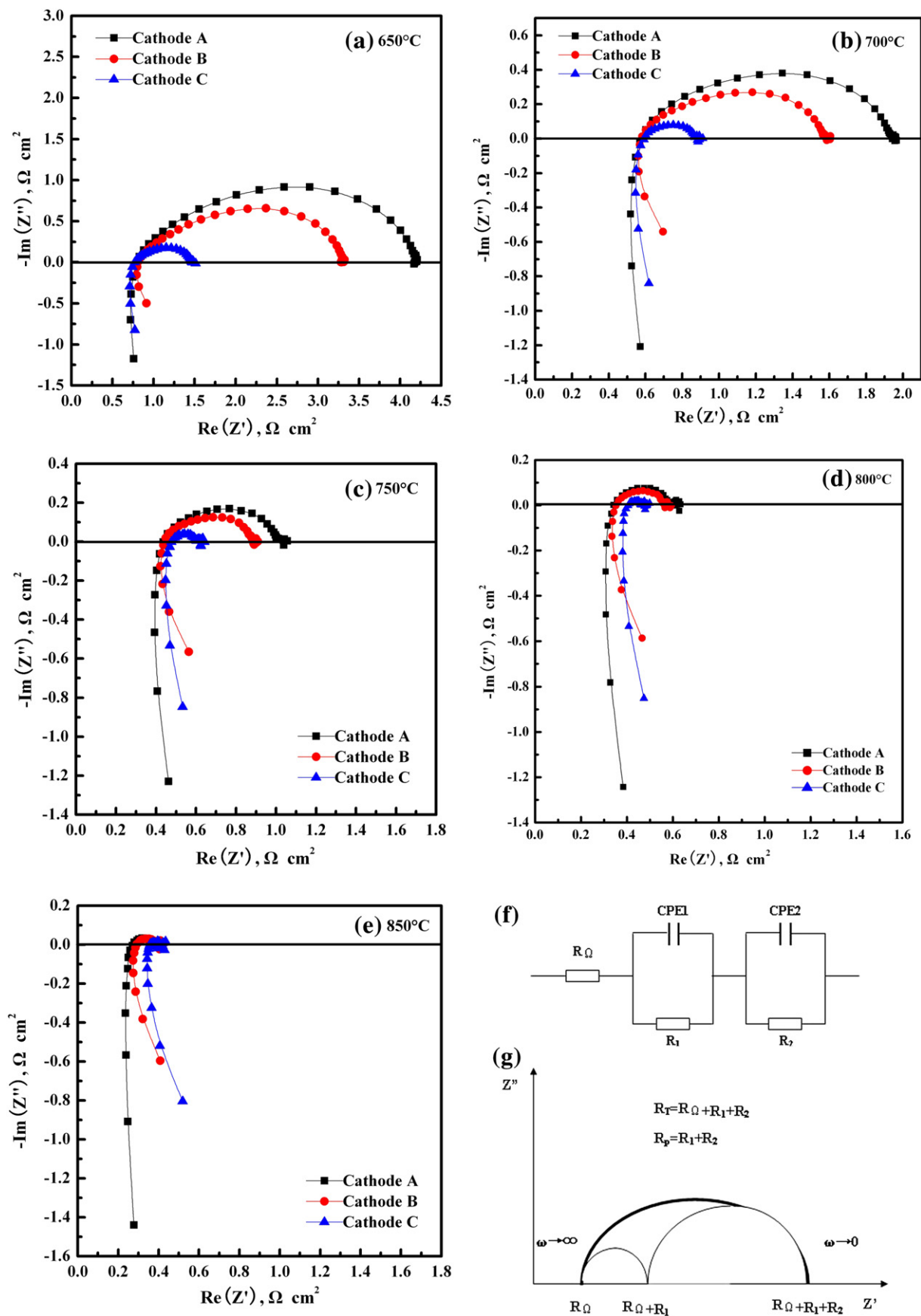
Fig. 4. Electrochemical impedance spectra of LNF-based cathodes measured at different temperatures in air: (a) 650 °C, (b) 700 °C, (c) 750 °C, (d) 800 °C and (e) 850 °C. EIS was measured at open circuit. (f) The equivalent circuit for data fitting. (g) Impedance sketch map on the complex plane.

Table 2
Total specific polarization resistance of LNF-based cathodes determined from Nyquist plots at different temperatures.

Specimens	650 °C R_P (Ω cm^2)	700 °C R_P (Ω cm^2)	750 °C R_P (Ω cm^2)	800 °C R_P (Ω cm^2)	850 °C R_P (Ω cm^2)
Cathode A	3.405	1.363	0.581	0.242	0.101
Cathode B	2.489	1.009	0.452	0.202	0.091
Cathode C	0.702	0.285	0.115	0.054	0.028

interpret the impedance curves of symmetrical cells, as shown in Fig. 4(f). Fig. 4(g) shows impedance sketch map on the complex plane. In the circuit, CPE and R denote constant phase element and cathode resistance, respectively. Generally, in solid cathode and electrolyte systems of the type studied here, the interface processes show considerable frequency dispersion. Such behavior is generally analyzed by the inclusion of a constant phase element. CPE can be expressed as follows, $Z_{CPE} = A(j\omega)^{-n}$, where ω is the angular frequency and $j = (-1)^{1/2}$ [49]. The values of n describe the fractal character (i.e. the heterogeneous or porous character) of the sample, the value of which is between 0 and 1 [50]. For $n = 0.5$, the CPE is a Warburg-type diffusion impedance and for $n = 1$, the CPE is a pure capacitance with $C = A^{-1}$. The high-frequency intercept of the impedance spectra corresponds to the specific ohmic resistance of the symmetric cell (R_Ω), including the ohmic resistance of the ScSZ electrolyte and GDC electrolyte, ohmic resistance of the cathode, contact resistance at the cathode/electrolyte interface and contact resistance between the cathodes and current collector Pt mesh. The low-frequency intercept gives the total specific resistance (R_T), which is the sum of the specific ohmic resistance of the cell (R_Ω) and the total specific polarization resistance (R_P) for the oxygen reduction reaction (ORR), including the effective specific interfacial polarization resistance corresponding to the electrochemical reactions at the cathode/electrolyte interface (R_1) and the specific concentration polarization resistance corresponding to mass-transfer or gas diffusion polarization (R_2). For the total specific polarization resistance, the resistance at high frequency is probably associated with charge transfer processes (R_1), which includes the electron-transfer and ion-transfer processes occurring at the current collector/cathode and cathode/electrolyte interfaces, respectively. The low-frequency arc can be attributed to the diffusion processes (R_2), which include adsorption–desorption of oxygen, oxygen diffusion at the gas/cathode surface interface, and surface diffusion of intermediate oxygen species [51–54]. The catalytic activity of the LNF-based cathodes, as characterized by the total specific cathode polarization resistance (R_P), was determined from the size of the impedance loop.

Fitting parameters for ORR on the LNF-based cathodes were listed in Tables 2 and 3. The specific polarization resistance R_p of cathode A were 0.101, 0.242, 0.581, 1.363, 3.405 Ω cm^2 at 850 °C, 800 °C, 750 °C, 700 °C and 650 °C, respectively. For cathode B, R_p was reduced to 0.091, 0.202, 0.452, 1.009, 2.489 Ω cm^2 at 850 °C, 800 °C, 750 °C, 700 °C and 650 °C, respectively. Notably, as for cathode C, R_p was further reduced to 0.028, 0.054, 0.115, 0.285, 0.702 Ω cm^2 at 850 °C, 800 °C, 750 °C, 700 °C and 650 °C,

respectively. We could find that cathode A revealed the largest R_p among the three cathode samples. In particular, cathode B exhibited an approximately 10–30% improvement in R_p, compared with cathode A. R_p of cathode C reduced approximately 70–80%, compared with cathode A. In addition, as shown in Table 3, the value of the gas phase diffusion resistance (R_2) is always noticeably larger than that of the charge transfer resistance (R_1). This implies that R_2 dominates the total specific cathode polarization resistance (R_p) at temperatures within the range of 650–850 °C. On the other hand, resistances (R_1 or R_2) gradually reduced from cathode A to cathode C. Evidently, with an increase in the number of cathode layers, there was a significant decrease in the total specific cathode polarization, implying a decrease in the impedance of ORR on the ScSZ electrolyte, i.e., the enhancement of electrochemical activity for the kinetics of ORR. Compared with composite LNF-based cathode (70 wt.% LNF–30 wt.% GDC), the functionally gradient LNF cathode with gradual changes in composite between ScSZ electrolyte and LNF cathode exhibited better adhesion resulting in the reduction in charge transfer resistance (R_1). Moreover, the decrease in gas phase diffusion resistance (R_2) may be associated with the area of triple phase boundaries (TPBs). The decrease in R_p for cathode B is mainly due to the gradual change rather than abrupt change in composition between ScSZ electrolyte and LNF cathode with dissimilar material structure. For the functionally gradient LNF cathode configuration, the compositions change gradually from one material to the other. Noticeably, the functionally gradient LNF composite cathode showed better performance in terms of its electrochemical properties compared with that of composite LNF-based cathode (70 wt.% LNF–30 wt.% GDC). Therefore, the functionally gradient cathode approach can be applied in the cathode/electrolyte interfaces of SOFC to improve cell performance. After impregnation, the impedance spectrum shape seemingly changed showing that both high- and low-frequency arcs were obviously reduced, indicating that both electrochemical processes (i.e. the electrochemical reactions at the cathode/electrolyte interface and adsorption–desorption of oxygen and/or oxygen diffusion at the gas–cathode interface) were simultaneously improved by active and nano-sized GDC particles. Investigation also indicates that the impregnation of nano-sized GDC greatly accelerates the oxygen dissociation and diffusion processes. The enhancement in oxygen reduction kinetics is most likely related to the high electrocatalytic effect and the high surface area of the impregnated nano-sized GDC phase [55]. The impregnation of the nano-sized ionic-conducting GDC phase in the predominantly electronic conducting LNF porous network could substantially enhance the TPBs for the ORR. This would be similar to the effect of GDC phase in the LSM/GDC composite cathodes on the promotion of the O_2 reduction reaction rate [56,57]. We could find that the LNF particles are covered with GDC particles that are at the nanoscale and can be as small as 40 nm (Fig. 3(b)). It is noted that impregnated GDC particles are connected, forming continuous pathway for oxygen ion conduction, and extending the TPB from the cathode/electrolyte interface to the bulk of the cathode. The microstructure evolution reveals that the advantage of the impregnation method compared to the conventional mechanically mixing method, at

Table 3
Fitting parameters for impedance spectra of LNF-based cathodes at different temperatures.

Specimens	650 °C		700 °C		750 °C		800 °C		850 °C	
	R_1 (Ω cm^2)	R_2 (Ω cm^2)	R_1 (Ω cm^2)	R_2 (Ω cm^2)	R_1 (Ω cm^2)	R_2 (Ω cm^2)	R_1 (Ω cm^2)	R_2 (Ω cm^2)	R_1 (Ω cm^2)	R_2 (Ω cm^2)
Cathode A	0.987	2.418	0.368	0.995	0.145	0.436	0.061	0.181	0.026	0.075
Cathode B	0.742	1.747	0.283	0.726	0.122	0.330	0.046	0.156	0.016	0.075
Cathode C	0.227	0.475	0.073	0.212	0.035	0.080	0.011	0.043	0.004	0.024

least partly, is the presence of fine particles which can generate much more TPBs, which result in the dramatic decrease in R_p. Most significantly, the cathode polarization performance of the GDC-impregnated LNF cathode is comparable to that of LSCF, $La_{0.8}Sr_{0.2}FeO_3$ (LSF) cathodes. LSCF is known to be a very good mixed ionic and electronic conductor with high electrocatalytic activity for the O_2 reduction reactions. The standard $La_{0.6}Sr_{0.4}Co_{0.8}Fe_{0.2}O_3$ and $La_{0.8}Sr_{0.2}Co_{0.8}Fe_{0.2}O_3$ material perform better than most materials, achieving a R_p of 0.31 and 0.3 Ω cm^2 at 700 °C, respectively [18,58]. As far as the R_p for cathodes on YSZ electrolyte is concerned, the cathode compositions with the highest performance are $La_{0.8}Sr_{0.2}FeO_3$ (LSF) and $La_{0.8}Sr_{0.2}Fe_{0.8}Co_{0.2}O_3$ (LSFC), which have R_p close to 0.1 Ω cm^2 and 0.3 Ω cm^2 at 700 °C, respectively [58]. However, the GDC-impregnated LNF cathode reported in this study shows comparable performance with those of the mixed ionic- and electronic-conducting (MIEC) cathodes.

Fig. 5 shows the activation energies of the specific cathode polarization resistance for three LNF-based cathode configurations. It was found that specific cathode polarization resistance (R_p) decrease dramatically with increasing temperature for three cathode samples. The activation energies of the specific cathode polarization resistance for LNF-based cathodes were in the range of 138.83–151.59 kJ mol^{-1}. These values are comparable to that of the $La_{0.8}Sr_{0.2}Co_{0.8}Fe_{0.2}O_3$ (LSCF) ($\sim$130 kJ mol^{-1}) cathode deposited on $Ce_{0.8}Sm_{0.2}O_{1.9}$ electrolyte reported in Ref. [59]. This suggests that LNF-based cathodes exhibit compatible activation energies of the specific cathode polarization resistance with that of LSCF cathode.

The activation energies of the specific cathode polarization resistance for cathode A, cathode B and cathode C were 151.59, 142.58 and 138.83 kJ mol^{-1}, respectively. Noticeably, the activation energy values for functionally gradient and GDC-impregnated LNF cathodes (cathode B and cathode C) both are lower than that of composite LNF-based cathode (cathode A). This implied that the two approaches would effectively improve the cathode performance. Especially for the GDC-impregnated LNF cathode (cathode C), its configurations with a continuous and three-dimensional networks could greatly accelerates the oxygen dissociation and diffusion processes, substantially enhance the triple phase boundaries for the ORR, thereby reducing in the activation energies of the specific cathode polarization resistance.

The exchange current density, i_0, which corresponds to the intrinsic ORR rate, is an important parameter for investigating oxygen reduction reaction mechanisms at the cathode [60]. The oxygen reduction reaction can be divided into several elemental steps: (1) diffusion of oxygen molecules in the gas phase to the cathode, (2) oxygen dissociate adsorption on the cathode surface, (3) surface diffusion of oxygen on the cathode, (4) incorporation of oxygen into the electrolyte via the triple phase boundary (TPB) and (5) oxide ion diffusion in the bulk of the cathode, and oxide ion transfer from cathode to electrolyte [61,62]. When the exchange current density is higher, the overpotential of the cathode is lower, suggesting that cathodes with higher exchange current density value exhibit higher performance in terms of electrochemical properties. The i_0 value can be obtained from the EIS. In this technique, i_0 is measured from the specific polarization resistance (R_p) of the Nyquist plot and calculated using Eq. (1) which is derived from the Bulter–Volmer equation [63]:

$$i_0 = \frac{RTv}{nFR_p} \tag{3}$$

Here, n is the total number of electrons passed in the reaction, v reflects the number of times the rate-determining step occurs for one occurrence of the full reaction, F is the Faraday constant ($F = 96,500$ C mol^{-1}), and R is the ideal gas constant ($R = 8.31$ J mol^{-1} K^{-1}). For the ORR, n and v are generally assumed to be 4 and 1, respectively (as the total number of electrons transferred per molecule of oxygen reduced is 4 and the rate-limiting step would likely have a stoichiometry of 1 for the oxygen reduction reaction) [59].

The i_0 values for the different structures of symmetric cell measured from Eq. (1) for EIS are given in Table 4, and their Arrhenius plots for i_0 values as a function of temperature are shown in Fig. 6. The linearity of the Arrhenius plots indicates that these LNF-based cathodes are stable as a function of temperature. At 850 °C, the i_0 values for cathode B and cathode C determined by the EIS were 265.86 and 864.03 mA cm^{-2}, respectively, both of which were larger than the i_0 value of 239.53 mA cm^{-2} for cathode A. From the slope of the line in the Arrhenius plots, the overall activation energy for the ORR was determined by the following equation.

$$\ln i_0 = \ln K - \frac{Ea}{RT} \tag{4}$$

where K is the pre-exponential constant, which can be calculated from the y-intercept, and Ea is the reaction activation energy [64]. The activation energy (Ea) for the ORR may be related to the structure of the cathode or to different cathode compositions. The ORR activation energies obtained from the slope of the Arrhenius plots were 160.09, 151.07 and 147.32 kJ mol^{-1} for cathode A, cathode B and cathode C, respectively. This suggests that the GDC-impregnated LNF and functionally gradient LNF cathode possessed the higher exchange current density (i_0) and the lower activation energy of the ORR, compared with composite LNF-based cathode (70 wt.% LNF–30 wt.% GDC), indicating that the ORR kinetics can be improved by using the configuration of a GDC-impregnated LNF and functionally gradient LNF cathode.

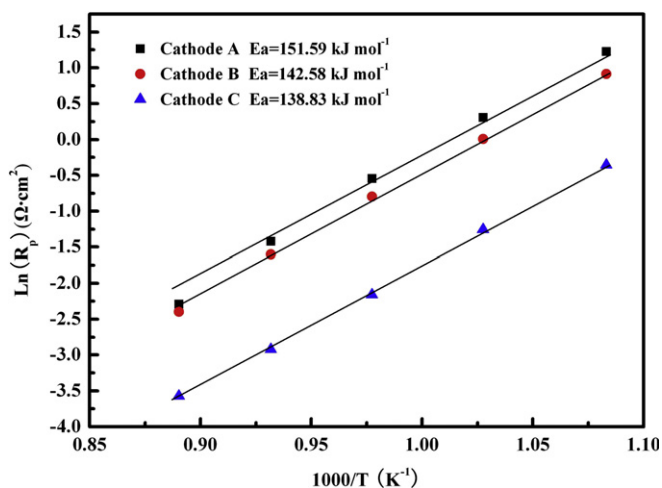**Fig. 5.** Arrhenius plots of the specific polarization resistance (R_p) for three different configurations of LNF-based cathodes.

Table 4
Exchange current density for the LNF-based cathodes using EIS technique in the temperature range of 650–850 °C.

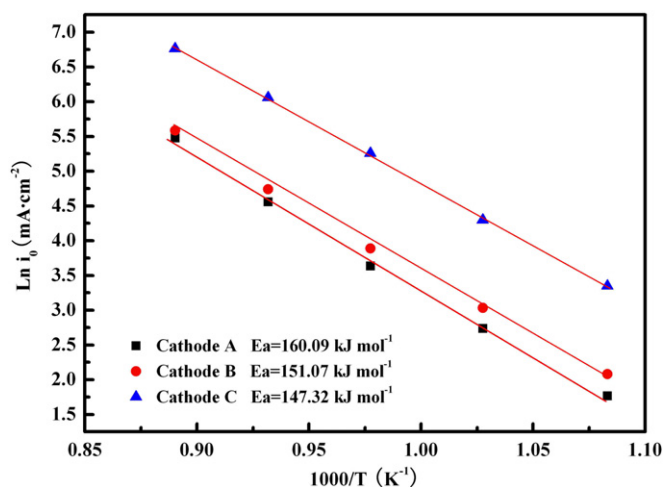| T (°C)	i_0 (mA cm^{-2})	i_0 (mA cm^{-2})	i_0 (mA cm^{-2})
	Cathode A	Cathode B	Cathode C
650	5.84	7.99	28.33
700	15.38	20.77	73.55
750	37.93	48.76	191.64
800	95.52	114.43	428.07
850	239.53	265.86	864.03

Fig. 6. Arrhenius plots of the exchange current density (i_0) as a function of temperature for the different structures of symmetric cell.

4. Conclusions

In this paper, $LaNi_{0.6}Fe_{0.4}O_3$-based cathodes with three different configurations (i.e. LNF–GDC composite cathode (70 wt.% LNF–30 wt.% GDC), functionally gradient LNF cathode and GDC-impregnated LNF cathode) were investigated to compare their electrochemical properties. The results revealed that the specific cathode polarization resistance (R_p) of LNF–GDC composite cathode (70 wt.% LNF–30 wt.% GDC) were 0.101, 0.242, 0.581, 1.363, 3.405 Ω cm^2 at 850 °C, 800 °C, 750 °C, 700 °C and 650 °C, respectively. R_p for functionally gradient LNF cathode was reduced to 0.091, 0.202, 0.452, 1.009, 2.489 Ω cm^2 at the same temperature, respectively. Notably, as for GDC-impregnated LNF cathode, R_p was further reduced to 0.028, 0.054, 0.115, 0.285, 0.702 Ω cm^2 at the same temperature, respectively. The functionally gradient cathode with gradual changes in composite between the cathode and electrolyte exhibited better adhesion resulting in the reduction in charge transfer resistance. Moreover, the decrease in gas phase diffusion resistance may be associated with the enhanced area of triple phase boundaries (TPBs). This implies that the functionally gradient cathode showed better performance in terms of its electrochemical properties compared to that of LNF–GDC composite cathode. The significant decrease in R_p was mainly attributed to the creation of electrolyte/cathode phase boundaries. As far as the GDC-impregnated LNF cathode is concerned, the impregnation of the nano-sized ionic conducting GDC phase in the predominantly electronic conducting LNF porous network could substantially enhance the TPBs, which result in the dramatic decrease in R_p. High electrochemical activity has been achieved for the oxygen reduction reaction (ORR) on the GDC-impregnated LNF cathodes. It was concluded that the GDC-impregnated LNF cathode possessed the lowest specific cathode polarization resistance (R_p), the lowest activation energies of the specific cathode polarization resistance and the lowest activation energy of the ORR among three cathode configurations. The impregnation approach may be applied in SOFC to improve its electrochemical properties.

Acknowledgements

References

[1] B.C.H. Steele, A. Heinzel, Nature 414 (2001) 345.
[2] T. Ishihara, J. Tabuchi, S. Ishikawa, J. Yan, M. Enoki, H. Matsumoto, Solid State Ionics 177 (2006) 1949.
[3] R. Polini, A. Falsetti, E. Traversa, O. Schäf, P. Knauth, J. Eur. Ceram. Soc. 27 (2007) 4291.
[4] R. Polini, A. Pamio, E. Traversa, J. Eur. Ceram. Soc. 24 (2004) 1365.
[5] Y.J. Leng, S.H. Chan, S.P. Jiang, K.A. Khor, Solid State Ionics 170 (2004) 9.
[6] T. Horita, K. Yamaji, M. Ishikawa, N. Sakai, H. Yokokawa, T. Kawada, J. Electrochem. Soc. 145 (1998) A3196.
[7] Z. Yang, K.S. Weil, D.M. Paxton, J.W. Stevenson, J. Electrochem. Soc. 150 (2003) A1188.
[8] K. Huang, P.Y. Hou, J.B. Goodenough, Solid State Ionics 129 (2000) 237.
[9] K. Hilpert, D. Das, M. Miller, D.H. Peck, R. Weiß, J. Electrochem. Soc. 143 (1996) 3642.
[10] M. Stanislowski, E. Wessel, K. Hilpert, T. Markus, L. Singheiser, J. Electrochem. Soc. 154 (2007) A295.
[11] B.J. Ingram, T.A. Cruse, M. Krumpelt, J. Electrochem. Soc. 154 (2007) B1200.
[12] D. Das, M. Miller, K. Hilpert, in: U. Bossel (Ed.), Proceedings of the First European Solid Oxide Fuel Cell Forum (3–7 October 1994, Lucerne, Switzerland), Druckerei J. Kinzelin, Gottingen, Germany, 1994, p. 703.
[13] H. Kurokawa, C.P. Jacobson, L.C. DeJonghe, S.J. Visco, Solid State Ionics 178 (2007) 287.
[14] S.P.S. Badwal, R. Deller, K. Foger, Y. Ramprakash, J.P. Zhang, Solid State Ionics 99 (3–4) (1997) 297.
[15] S. Taniguchi, M. Kadowaki, H. Kawamura, T. Yasuo, Y. Akiyama, Y. Miyake, T. Saitoh, J. Power Sources 55 (1995) 73.
[16] S.P. Jiang, S. Zhang, Y.D. Zhen, J. Electrochem. Soc. 153 (2006) A127.
[17] S.P. Jiang, J.P. Zhang, L. Apateanu, K. Foger, J. Electrochem. Soc. 148 (2001) C447.
[18] S.P. Jiang, Solid State Ionics 146 (2002) 1.
[19] San Ping Jiang, Yongda Zhen, Solid State Ionics 179 (2008) 1459.
[20] S.P. Jiang, J.P. Zhang, X.G. Zheng, J. Eur. Ceram. Soc. 22 (2002) 361.
[21] R. Chiba, F. Yoshimura, Y. Sakurai, Solid State Ionics 124 (1999) 281.
[22] R. Chiba, F. Yoshimura, Y. Sakurai, Solid State Ionics 152 (2002) 575.
[23] G.Y. Laua, M.C. Tucker, C.P. Jacobson, S.J. Visco, S.H. Gleixner, L.C. DeJonghe, J. Power Sources 195 (2010) 7540.
[24] S. Li, J. Sun, X. Sun, B. Zhu, Electrochem. Solid-State Lett. 9 (2006) A86.
[25] H. Orui, K. Watanabe, R. Chiba, M. Arakawa, J. Electrochem. Soc. 151 (9) (2004) A1412.
[26] Manuela Bevilacqua, Tiziano Montini, Claudio Tavagnacco, Emiliano Fonda, Paolo Fornasiero, Mauro Graziani, Chem. Mater. 19 (2007) 5926.
[27] A. Weber, R. Manner, E. Ivers-Tiffee, Denki Kagaku 64 (1996) 582.
[28] E. Ivers-Tiffee, Andre Webe, Klaus Schmid, Volker Krebs, Solid State Ionics 174 (2004) 223.
[29] S.I. Hashimoto, K. Kammer, P.H. Larsen, F.W. Poulsen, M. Mogensen, Solid State Ionics 176 (2005) 1013.
[30] M. Bevilacqua, T. Montini, C. Tavagnacco, G. Vicario, P. Fornasiero, M. Graziani, Solid State Ionics 177 (2006) 2957.
[31] P.N. Dyer, R.E. Richards, S.L. Russck, D.M. Taylor, Solid State Ionics 134 (2000) 21.
[32] J.P.P. Huijsmans, F.P.F. Van Berkel, G.M. Christie, J. Power Sources 71 (1998) 107.
[33] B.C.H. Steele, K.M. Hori, S. Uchino, Solid State Ionics 135 (2000) 445.
[34] W. Zhou, Z. Shao, R. Ran, P. Zeng, H. Gu, W. Jin, N. Xu, J. Power Sources 168 (2007) 330.
[35] B.C.H. Steele, Solid State Ionics 75 (1995) 157.
[36] B. Steele, Solid State Ionics 86–88 (1996) 1223.
[37] R. Doshi, V.L. Richards, J. Carter, X. Wang, M. Krumpelt, J. Electrochem. Soc. 146 (1999) 1273.
[38] U.G. Bossel, Facts and Figures, Swiss Federal Office of Energy, Berne, Switzerland, 1992.
[39] M. Koizumi, Am. Ceram. Soc. 34 (1993) 3.
[40] Y. Huang, K. Ahn, J.M. Vohs, R.J. Gorte, J. Electrochem. Soc. 151 (2004) A1592.
[41] T.Z. Sholklapper, C. Lu, C.P. Jacobson, S.J. Visco, L.C. De Jonghe, Electrochem. Solid-State Lett. 9 (2006) A376.
[42] M. Shah, S.A. Barnett, Solid State Ionics 179 (2008) 2059.
[43] J.M. Vohs, R.J. Gorte, Adv. Mater. 21 (2009) 943.
[44] Bo Huang, Xin-jian Zhu, Yao Lv, Heng Liu, J. Power Sources 209 (2012) 209.
[45] Z.P. Shao, S.M. Haile, Nature 431 (2004) 170.
[46] S. Jain, K. Adiga, V. Vrneker, Combust. Flame 40 (1981) 71.
[47] H.J. Hwang, J.W. Moon, J. Moon, M. Awano, J. Am. Ceram. Soc. 88 (2005) 79.
[48] H.J. Hwang, J.W. Moon, S. Lee, E.A. Lee, J. Power Sources 145 (2005) 243.
[49] S.P. Jiang, J.G. Love, S.P.S. Badwal, Key Eng. Mater. 125–126 (1997) 81.
[50] J.X. Zhu, D.F. Zhou, S.R. Guo, J.F. Ye, X.F. Hao, X.Q. Cao, J. Meng, J. Power Sources 174 (2007) 114.
[51] W. Zhou, R. Ran, Z. Shao, R. Cai, W. Jin, N. Xu, J. Ahn, Electrochim. Acta 53 (2008) 4370.
[52] S.B. Adler, Solid State Ionics 135 (2000) 603.
[53] C. Fu, K. Sun, N. Zhang, X. Chen, D. Zhou, Electrochim. Acta 52 (2007) 4589.
[54] F. Qiang, K.N. Sun, N.Q. Zhang, X.D. Zhu, S.R. Le, D.R. Zhou, J. Power Sources 168 (2007) 338.
[55] San Ping Jiang, Wei Wang, J. Electrochem. Soc. 152 (7) (2005) A1398.

[56] E.P. Murray, S.A. Barnett, Solid State Ionics 143 (2001) 265.
[57] Y.N. Kim, A. Manthiram, J. Electrochem. Soc. 158 (10) (2011) B1206.
[58] J.M. Ralph, A.C. Schoeler, M. Krumpelt, J. Mater. Sci. 36 (2001) 1161.
[59] J. Liu, A.C. Co, B. Paulson, V.I. Briss, Solid State Ionics 177 (2006) 377.
[60] S.B. Adler, Chem. Rev. 104 (2004) 4791.

[61] M. Kleitz, F. Petitbon, Solid State Ionics 92 (1996) 65.
[62] A. Ringuede, J. Fouletier, Solid State Ionics 139 (2001) 167.
[63] J. Piao, K. Sun, N. Zhang, X. Chen, S. Xu, D. Zhou, J. Power Sources 172 (2007) 633.
[64] A.C. Co, S.J. Xia, V.I. Briss, J. Electrochem. Soc. 152 (2005) A570.